International Journal of Infrared and Millimeter Waves (2020) 41:1009–1021
https://doi.org/10.1007/s10762-020-00716-z

Characterization of the Observed Electric Field and Molecular Relaxation Times for Millimeter-Wave Chirped Pulse Instrumentation

G. Dhont[1] · D. Fontanari[1] · C. Bray[1] · G. Mouret[1] · A. Cuisset[1] · F. Hindle[1] · K. M. Hickson[2] · R. Bocquet[1]

Received: 14 February 2020 / Accepted: 1 June 2020 / Published online: 1 July 2020

Abstract
In a chirped pulse experiment, the strength of the signal level is proportional to the amplitude of the electric field, which is weaker in the millimeter-wave or submillimeter-wave region than in the microwave region. Experiments in the millimeter region thus require an optimization of the coupling between the source and the molecular system and a method to estimate the amplitude of the electric field as seen by the molecular system. We have developed an analytical model capable of reproducing the coherent transient signals obtained with a millimeter-wave chirped pulse setup operated in a monochromatic pulse mode. The fit of the model against the experimental data allowed access to the amplitude of the electric field and, as a byproduct, to the molecular relaxation times T_1 and T_2.

Keywords Chirped pulse · Coherent transients · Polarization · Relaxation time · Rabi frequency · Bloch equations

1 Introduction

Recent developments in electronics allow the realization of new kinds of experiments which were difficult to perform during the previous millennium [1–5]. In particular the existence of arbitrary wave generators in the microwave region associated with amplified frequency multiplier chains and high-speed giga-sampling oscilloscopes make it possible to shape any type of electromagnetic pulse with a time precision of the order of a nanosecond. These improvements in microwave and millimeter-wave

✉ G. Dhont
guillaume.dhont@univ-littoral.fr

[1] LPCA, Université du Littoral Côte d'Opale, 189A avenue Maurice Schumann, 59140 Dunkerque, France

[2] ISM, Université de Bordeaux, 351 cours de la libération, 33405 Talence cedex, France

sources allow the design of chirped pulse (CP) experiments routinely used nowadays in high resolution rotational molecular spectroscopy. They allow the bandwidth and available power of modern millimeter sources to be exploited. High instrument sensitivity is achieved by efficient averaging of many cycles made possible by the phase repeatable pulses and the coherent nature of the molecular reemission. This gives experiments able to provide a rotational spectrum over a few tens of GHz in a minute. On the other hand, the nanosecond temporal accuracy of CP gives access to kinetic or transient experiments [6]. In the millimeter-wave and submillimeter-wave ranges [3, 4, 7], the source power is often weak, suggesting the use of slow CPs to enhance the signal. The drawback in this case is the dependence of the line intensity on its temporal position within the pulse. However, a heuristic correction to this problem has been proposed by our group [8].

A typical CP measurement cycle consists of two steps. In the first step, a gas sample is polarized by the CP. In the second step, the source is switched off and the emission of the molecules, corresponding to the Free Induction Decay (FID) signal, is recorded. The spectrum of the molecular emission is then recovered by the use of a Fourier transform. The polarization of the sample reached at the end of the CP and thus the Free Induction Decay signal depends on the Rabi frequency $\Omega_0 = \frac{\mu_{ab} E_0}{\hbar}$, where μ_{ab} is the transition dipole moment and E_0 the electric field amplitude seen by the molecular system [8–10].

In most millimeter-wave CP experiments, the electromagnetic field felt by the molecular system is not amplified by a resonant cavity unlike experiments in the 1980s for which molecular beams were coupled to resonant cavities [11–13]. At millimeter wavelengths, the available power is limited by the power handling capacity of the frequency multipliers. A technique to characterize and optimize the electric field observed by the molecular system at these frequencies is then desirable.

Park et al. [4] proposed to measure the source power coupling by using coherent transients experiments. It consists of exciting a transition with a resonant single-frequency pulse and recording the amplitude of the FID signal as a function of the pulse duration. They use a molecular beam expansion under collision-free conditions which allows them to neglect the relaxation time of the population difference T_1. The resulting characteristic of the FID signal is a damped oscillation driven by the Rabi frequency (see Eq. (1) of [4]). The first maximum can be considered as a "$\frac{\pi}{2}$ pulse" [14] and would be a direct image of the amplitude of the electromagnetic field seen by the molecular system. In our experiment [7], we are not dealing with a molecular beam and our data does not fit the model used by Park et al. This motivated us to develop a model which takes into account the two relaxation times T_1 and T_2 in order to reproduce the coherent transient signals obtained with our millimeter-wave CP instrument operated in a monochromatic pulse mode. We are then able to evaluate the Rabi frequency Ω_0 and the amplitude of the electric field E_0 using a least squares procedure. The data analysis gives access as a byproduct to the molecular relaxation times T_1 and T_2. It comes as an alternative to previous experimental methods that fully characterize the dynamics of molecular systems, i.e., to measure jointly the relaxation times of populations (T_1) and phases (T_2): coupling of pump-probe techniques and photon echoes in the condensed phase [15], femtosecond time-resolved four-wave mixing experiments in the diluted phase [16]. Older experiments on optical

nutation, optical precession and photon echoes in the mm-wave domain have also been performed more than 40 years ago by a few groups (e.g., [10, 14, 17]).

2 Experimental Setup

The experimental setup in Fig. 1 has been described in detail in a precedent publication [7]. The excitation source is an amplified multiplier chain (AMC, Virginia

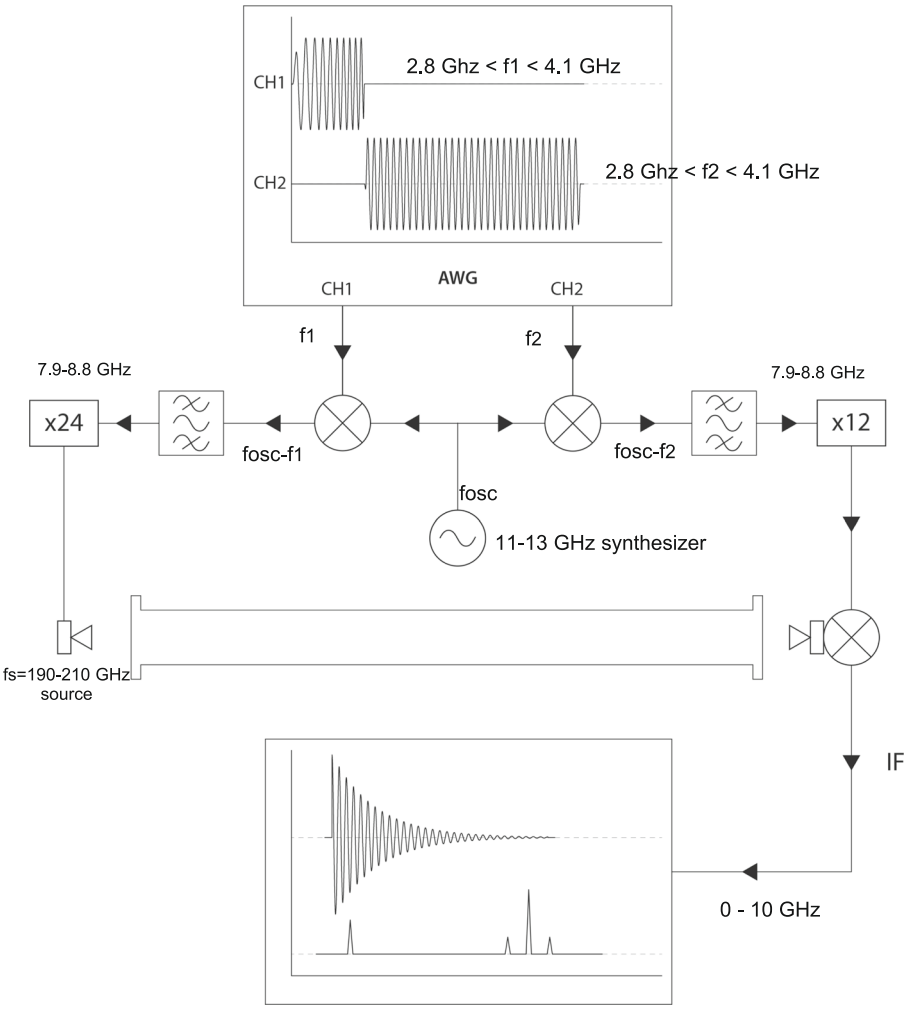

Fig. 1 Millimetre wave chirped pulse instrument. Emission of a chirped pulse in the range 190 to 210 GHz generated at microwave frequency by the first channel of the arbitrary wave generator. The pulse is propagated through a measurement cell allowing the interaction with a gaseous sample. The Free Induction Decay signal after the pulse is measured using an heterodyne detection scheme and a high-speed oscilloscope

Diodes Inc.) that has an overall frequency multiplication factor of 24. An input frequency range of 7.9–8.7 GHz to the AMC linearly addresses the final frequency output range of 190–210 GHz. The output power is 30–50 mW across the 190–210 GHz frequency range. Chirped pulse generation uses a high-speed (12 GS/s) arbitrary waveform generator (AWG, Tektronix 7122C). Waveforms, in the frequency range of 2.0–3.5 GHz, are created by the AWG. They are upconverted to the required 7.9–8.7 GHz AMC input range by mixing with a synthesizer operating at a fixed frequency between 9 and 12 GHz. The upper sideband is selected by a bandpass filter and amplified to ensure the RF input power complies with safe operation of the AMC. The time and frequency scales of all instruments are derived from a GPS timing signal distributed locally via a 10 MHz carrier.

3 Theory

3.1 From a 2-Level System to Optical Bloch Equations

The molecular interaction with an electromagnetic wave has been extensively described in the literature [9, 18–20]. We discuss for simplicity a two-level isolated molecular system, given by its energy levels E_a and E_b with $E_a - E_b = \hbar\omega_0$. We consider the interaction between the electric dipole moment of this 2-level system and an electric field with angular frequency $\omega(t)$ given by

$$E(y,t) = \frac{1}{2}E_0 e^{-i[\omega(t)t-ky]} + cc. \tag{1}$$

The evolution of the system is described by the evolution of its density matrix. Introducing relaxation mechanisms by $\gamma_1 = \frac{1}{T_1}$ and $\gamma_2 = \frac{1}{T_2}$ (respectively, the inverse of the decay time of the population difference and the inverse of the dipole dephasing time), W_{eq} the population difference at thermodynamic equilibrium, we get the generic form of the optical Bloch equations [8] (see Appendix 1):

$$\begin{cases} \dfrac{dz}{dt} = -(\gamma_2 + i\omega_0)z(t) - i\mathcal{E}(t)W(t) \\ \dfrac{dW}{dt} = -\gamma_1(W(t) - W_{eq}) + \dfrac{1}{2i}(\mathcal{E}(t)^* z(t) - \mathcal{E}(t)z(t)^*) \end{cases}, \tag{2}$$

where $W(t)$ and $z(t) = \mathcal{P}(t)/(N\mu_{ab})$ correspond to the difference of population and the pseudopolarization, respectively, with $\mathcal{P}(t)$ being the polarization. $\mathcal{E}(t) = e^{-i\alpha(t)}\Omega_0$ is a complex-valued function representing the interaction of the dipole moment with the electric field, where $\Omega_0 = \frac{\mu_{ab}E_0}{\hbar}$ is the Rabi frequency and $\alpha(t)$ a generic function of time [8].

3.2 Bloch Equations in the "Rotating Frame"

We define a new variable $\xi(t) = e^{i\alpha(t)}z(t)$ to simplify the equations of motion, corresponding to the rotating frame. We introduce the detuning from the resonant frequency by $\delta(t) = \omega_0 - \frac{d\alpha}{dt}$. Equation (2) becomes:

$$\begin{cases} \dfrac{d\xi}{dt} = -[\gamma_2 + i\delta(t)]\,\xi(t) - i\Omega_0(t)W(t) \\ \dfrac{dW}{dt} = -\gamma_1(W(t) - W_{eq}) + \dfrac{\Omega_0(t)}{2i}(\xi(t) - \xi(t)^*) \end{cases}. \tag{3}$$

Let $\xi(t) = \hat{U}(t) - i\hat{V}(t)$ to get the optical Bloch equations in the "rotating frame"

$$\begin{cases} \dfrac{d\hat{U}}{dt} = -\gamma_2\hat{U}(t) - \delta(t)\hat{V}(t) \\ \dfrac{d\hat{V}}{dt} = -\gamma_2\hat{V}(t) + \delta(t)\hat{U}(t) + \Omega_0(t)W(t) \\ \dfrac{dW}{dt} = -\gamma_1(W(t) - W_{eq}) - \Omega_0(t)\hat{V}(t) \end{cases}. \tag{4}$$

3.3 Monochromatic Source—Coherent Transients

The molecular polarization in the case of the linear CP has been studied in a recent publication [8]. Here, we are dealing with the source at a fixed frequency to measure the Rabi frequency and then deduce the electric field E_0 seen by the molecular system. We consider the case $\alpha(t) = (\omega_0 - \delta)t$ (δ, the "detuning," is a constant), the initial conditions $U(0) = V(0) = 0$ (non polarized molecules) and $W(0) = W_{eq}$ (thermalized sample). The system of differential equations (4) is then linear with constant coefficients and has the form

$$\frac{d\mathbf{X}(t)}{dt} = \mathsf{A}\mathbf{X}(t) + \mathbf{b}, \tag{5}$$

where $\mathbf{X}(t) = (U(t), V(t), W(t))^T$ is the Bloch vector, $\mathbf{b}(t) = (0, 0, W_{eq}\gamma_1)^T$, and

$$\mathsf{A} = \begin{pmatrix} -\gamma_2 & -\delta & 0 \\ \delta & -\gamma_2 & \Omega_0 \\ 0 & -\Omega_0 & -\gamma_1 \end{pmatrix}. \tag{6}$$

The solution of the system is given by

$$\mathbf{X}(t) = \exp(t\mathsf{A})(\mathbf{X}(0) + \mathsf{A}^{-1}\mathbf{b}) - \mathsf{A}^{-1}\mathbf{b}. \tag{7}$$

The components of $\mathbf{X}(t)$ are linear combinations of $e^{\lambda_i t}$ plus a constant term, with λ_i, $i = 1, 2, 3$, eigenvalues of A. In particular, taking into account our initial conditions, we have:

$$X_i(t) = a_1e^{\lambda_1 t} + a_2e^{\lambda_2 t} + a_3e^{\lambda_3 t} - (a_1 + a_2 + a_3) + X_i(0). \tag{8}$$

The general solution, involving the eigenvalues and eigenstates of a 3×3 matrix, is complicated. We can however compute the equilibrium state $\mathbf{X}(\infty)$ defined by

$$\mathsf{A}\mathbf{X}(\infty) + \mathbf{b} = \mathbf{0}, \tag{9}$$

that is

$$\begin{cases} U(\infty) = -\dfrac{T_2^2 \delta \Omega_0 W_{eq}}{1 + T_2^2\delta^2 + T_1 T_2 \Omega_0^2} \\ V(\infty) = \dfrac{T_2 \Omega_0 W_{eq}}{1 + T_2^2\delta^2 + T_1 T_2 \Omega_0^2} \\ W(\infty) = \dfrac{(1 + T_2^2\delta^2) W_{eq}}{1 + T_2^2\delta^2 + T_1 T_2 \Omega_0^2} \end{cases} \tag{10}$$

3.3.1 Resonant Case

For the resonant case, $\delta = 0$, i.e., when the exciting field has the same frequency as the transition of the 2-level system, $U(t)$ is decoupled from the other variables. Taking the same initial conditions, $U(t) = 0$ and the two eigenvalues that drive the dynamics of V and W are $\lambda_\pm = -\gamma_+ \pm i\Delta$ where

$$\begin{cases} \gamma_\pm = \dfrac{\gamma_1 \pm \gamma_2}{2} \\ \Delta = \sqrt{\Omega_0^2 - \gamma_-^2} \end{cases} \tag{11}$$

so that

$$\begin{cases} V(t) = e^{-\gamma_+ t}(\rho_c \cos(\Delta\, t) + \rho_s \sin(\Delta\, t)) - \rho_c \\ W(t) = e^{-\gamma_+ t}(\sigma_c \cos(\Delta\, t) + \sigma_s \sin(\Delta\, t)) - \sigma_c + W_{eq} \end{cases} \tag{12}$$

This is an expression appropriate for Δ real, i.e., $\Omega_0 \geq \gamma_-$. Otherwise, Δ should be chosen as $\Delta = \sqrt{\gamma_-^2 - \Omega_0^2}$ and the trigonometric functions in the expressions for $V(t)$ and $W(t)$ should be replaced by their corresponding hyperbolic functions. Through diagonalization of A it is possible to find explicit expressions for $\rho_{c,s}$ and $\sigma_{c,s}$ parameters,

$$\begin{aligned} \rho_c &= -\frac{\gamma_+ + \gamma_-}{\Delta^2 + \gamma_+^2} W_{eq} \Omega_0 \\ \rho_s &= \frac{\Delta^2 - \gamma_+\gamma_-}{\Delta\left(\Delta^2 + \gamma_+^2\right)} W_{eq} \Omega_0 \\ \sigma_c &= \frac{\Delta^2 + \gamma_-^2}{\Delta^2 + \gamma_+^2} W_{eq} \\ \sigma_s &= \frac{\Delta^2 + \gamma_-^2}{\Delta(\Delta^2 + \gamma_+^2)} W_{eq} \gamma_+ \end{aligned} \quad . \tag{13}$$

4 Comparison with Experimental Data

Our experiments are performed in the resonant case. We measure the FID signal $S(t)$ which is proportional to $V(T_p)$ given by Eq. (12) where T_p is the pulse duration. Neglecting the Doppler effect, the FID signal can be written as [8]:

$$S(t) = \left[e^{-\gamma_+ T_p}(\hat{\rho}_c \cos(\Delta\, T_p) + \hat{\rho}_s \sin(\Delta\, T_p)) - \hat{\rho}_c\right] \mathrm{e}^{-\gamma_2 t} \cos\left(\omega_{IF} t + \varphi\right), \quad (14)$$

where ω_{IF} is the intermediate frequency corresponding to the resonant molecular frequency and $\left(\hat{\rho}_c, \hat{\rho}_s\right) = C\left(\rho_c, \rho_s\right)$ are experimental quantities for some $C > 0$. By applying a Fast Fourier Transform on the FID signal, we are able to recover the amplitude $V(T_p)$. We recorded this amplitude versus the pulse duration to get the curve $V(T_p)$ (see Fig. 2). We then applied a least squares procedure against the model of Eq. (12) to fit the parameters Δ, $\hat{\rho}_c$, $\hat{\rho}_s$ and γ_+. The other parameters can be written as:

$$\begin{aligned} \gamma_- &= \frac{\hat{\rho}_c \Delta + \hat{\rho}_s \gamma_+}{\hat{\rho}_c \gamma_+ - \hat{\rho}_s \Delta} \Delta \\ C &= \frac{\Delta \hat{\rho}_s - \gamma_+ \hat{\rho}_c}{W_{eq}\, \Omega_0} \end{aligned} . \quad (15)$$

The absolute value of Ω_0 can be obtained from the relationship $\Omega_0^2 = \Delta^2 + \gamma_-^2$. Using the value of μ_{ab}, it is then immediate to recover the values of E_0, $T_1 = 1/\gamma_1$ and $T_2 = 1/\gamma_2$.

We studied the rotational transition $J = 17 \rightarrow 16$ of the OCS molecule at the frequency $\nu_0 = 206.745$ GHz, for which the Doppler line width is 160 kHz (HWHM) at 300 K. We recorded the FID signals obtained after an excitation pulse at the resonant frequency ν_0 for different pulse durations T_p and different gas pressures. Figure 2 shows the comparison between the amplitude of the experimental FID signals and the fit of Eq. (12) for 10 µbar, 50 µbar and 200 µbar of OCS pressure. The validity of the model is checked by comparing the fitted T_2 relaxation times with previous data based on collisional self-broadening measurements in the spectral domain [21]. We find that the model fits well the experimental data as soon as the gas pressure is higher than 50 µbar. For 10 µbar, the Doppler line broadening is larger than the collisional broadening (50 kHz) suggesting that our model which neglects the Doppler effect is insufficient. We attempted to develop a model to take into account the Doppler effect but the fit procedures did not converge correctly and therefore could not bring any improvement on the fitted parameters. We have therefore decided to retain the model presented here keeping in mind that the Doppler broadening must be negligible against the collisional one. This limitation is experimentally easy to respect. Table 1 summarizes the fit results where the first line gives the HWHM of the collisional broadening and the second line, the theoretical value of T_2, both using the self collisional broadening of the OCS line taken from ref. [21].

The electric field polarizing the molecular system can be determined using $\Omega_0 = \frac{\mu_{ab} E_0}{\hbar}$ where the value of $\mu_{ab} = 0.3$ D is calculated as described in Appendix 2. Taking $\Omega_0 = 3.3$ MHz from an averaging of fitted values for 50 µbar and 200 µbar, we

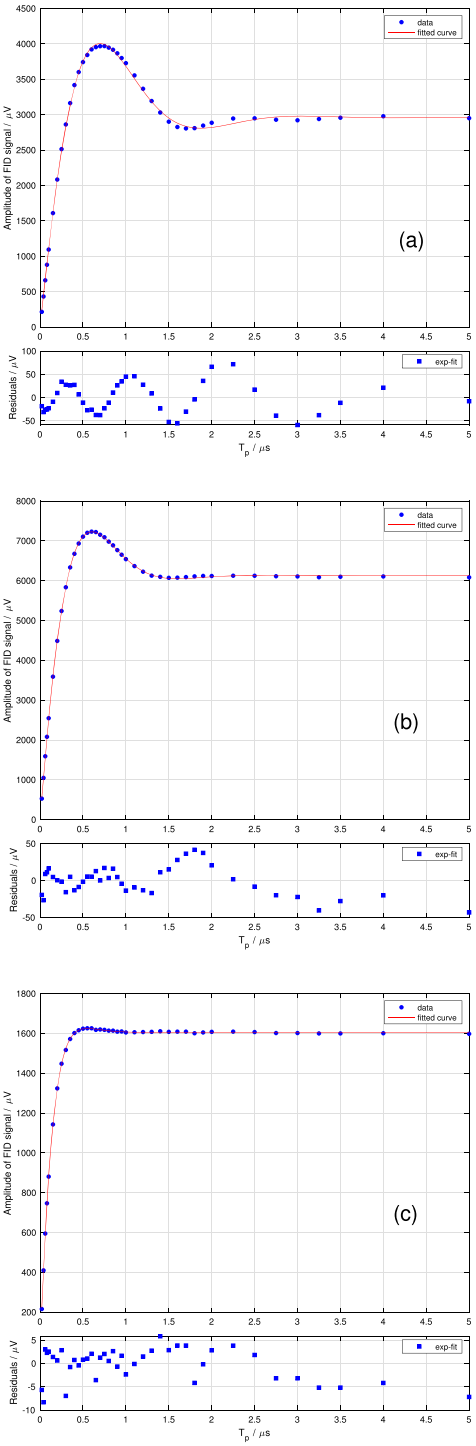

Fig. 2 Amplitude of the FID signal as a function of the pulse duration T_p for the $J = 17 \rightarrow 16$ rotational transition of the OCS molecule at the frequency $\nu_0 = 206.745$ GHz at three different OCS pressures: **a** 10 µbar, **b** 50 µbar and **c** 200 µbar. Dots are experimental data, curves are the fits using the model of Eq. (14) and squares are the residuals

Table 1 Calculated (see text) and fitted parameters of OCS for the $J = 17 \rightarrow 16$ rotational transition at $\nu_0 = 206.745$ GHz.

OCS: $J = 17 \rightarrow 16$, $\nu_0 = 206.745$ GHz				
Parameters	Type	P (μbar)		
		10	50	200
$\Delta\nu_{\text{coll}}$ (MHz)	Calculated	0.047	0.235	0.94
T_2 (μs)		2.9	0.6	0.15
$T_{2\text{exp}}$ (μs)	Fitted	1.2 ± 0.3	0.638 ± 0.007	0.173 ± 0.004
$T_{1\text{exp}}$ (μs)		0.40 ± 0.03	0.2670 ± 0.0008	0.1360 ± 0.0001
$\Omega_{0\text{exp}}$ (MHz)		2.8 ± 0.1	3.33 ± 0.05	3.4 ±0.2

find $E_0 = 3.75\,\text{V cm}^{-1}$. We use a 30 mW source. Considering ref. [22], the conversion value between the electric field and the power is $\left[\frac{E_0}{\text{V cm}^{-1}}\right] = 27.45\sqrt{\left[\frac{P}{\text{W cm}^{-2}}\right]}$. We calculate the theoretical value of the electric field, assuming a perfect coupling of the source and a 1 cm beam diameter, to get $E_{0\text{th}} = 5.36\,\text{V cm}^{-1}$. We can then estimate a coupling ratio $\frac{E_0}{E_{0\text{th}}}$ of 70% in our experiment which is equivalent to a 50% power coupling efficiency.

5 Conclusion

We show that the model established for the polarization in the case of a monochromatic source is able to reproduce the data obtained if the gas pressure is sufficiently high to be able to neglect Doppler broadening. The model takes into account the two relaxation times T_1 and T_2 which can then be determined by the fit procedure. It is also well suited to determine the electric field seen by the molecular system by fitting the Rabi frequency. Using only those measurements for which Doppler broadening is negligible compared with collisional broadening, we were able to establish that 70% of the source electric field amplitude was coupled to the molecular system.

Acknowledgments We would like to thank the Calculco cluster of the Université du Littoral Côte d'Opale for the use of software facilities. We thank the editor and the referees for their work during the COVID-19 pandemia.

Funding Information This work received financial support from the French Agence Nationale de la Recherche via funding of the project Original Sub-millimetre Chirped pulse instrumentation for Astrochemical Reactivity (OSCAR) under contract number ANR-15-CE29-0017. This work also received financial support from the Région Hauts-de-France, the Ministère de l'Enseignement Supérieur et de la Recherche (CPER Climibio), and the European Fund for Regional Economic Development through the TERAFOOD project (INTERREG V FR-WA-VL 1.2.11).

Appendix 1. Optical Bloch Equations

To establish the optical Bloch equations, we consider a two isolated level system ($|a\rangle$, $|b\rangle$) given by their energy level E_a and E_b with $E_a - E_b = \hbar\omega_0$. The system is subjected to a pulsed electromagnetic field, polarized parallel to Oz, propagating following Oy, with an angular frequency $\omega(t)$ which can be a function of time as in the chirped pulse experiment. $|a\rangle$ and $|b\rangle$ are eigenstates for H_0 and $\mathcal{E}(t)$ is a complex-valued function representing the perturbation of the system.

Description of the System

$$\begin{aligned}
\langle a|H_0|a\rangle &= \frac{E_a + E_b}{2} + \frac{\hbar\omega_0}{2},\\
\langle b|H_0|b\rangle &= \frac{E_a + E_b}{2} - \frac{\hbar\omega_0}{2},\\
\langle a|V(t)|b\rangle &= -\frac{\hbar}{2}\mathcal{E}(t),\\
\langle a|V(t)|a\rangle &= \langle b|V(t)|b\rangle = 0.
\end{aligned} \tag{16}$$

The hamiltonian of the system is then given by:

$$H = H_0 + V(t) = \begin{bmatrix} \frac{E_a+E_b}{2} + \frac{\hbar\omega_0}{2} & -\frac{\hbar}{2}\mathcal{E}(t) \\ -\frac{\hbar}{2}\mathcal{E}(t)^* & \frac{E_a+E_b}{2} - \frac{\hbar\omega_0}{2} \end{bmatrix} \tag{17}$$

The system can be described by the density matrix $\rho(t)$. From its diagonal and off-diagonal elements, the time dependent functions $W(t)$ and $z(t)$ corresponding to the difference of population and the pseudo polarization ($z(t) = \frac{\mathcal{P}(t)}{N\mu_{ab}}$) are defined as:

$$\begin{aligned}
W(t) &= \langle a|\rho(t)|a\rangle - \langle b|\rho(t)|b\rangle,\\
z(t) &= 2\langle a|\rho(t)|b\rangle.
\end{aligned} \tag{18}$$

Taking into account that its trace is unity, we get:

$$\begin{cases} \langle a|\rho(t)|a\rangle - \langle b|\rho(t)|b\rangle = & W(t) \\ \langle a|\rho(t)|a\rangle + \langle b|\rho(t)|b\rangle = & 1 \end{cases} \Rightarrow \begin{cases} 2\langle a|\rho(t)|a\rangle = & 1 + W(t) \\ 2\langle b|\rho(t)|b\rangle = & 1 - W(t) \end{cases}. \tag{19}$$

Finally, taking into account that the density matrix is hermitian, we can write it as:

$$\rho(t) = \frac{1}{2}\begin{pmatrix} 1 + W(t) & z(t) \\ z(t)^* & 1 - W(t) \end{pmatrix}, \tag{20}$$

where the asterisk denotes the complex conjugate.

Evolution of the System

The evolution of the system is driven by the Von Neumann equation:

$$\frac{d\rho}{dt} = \frac{-i}{\hbar}[H(t), \rho(t)]. \tag{21}$$

Developing the commutator of the hamiltonian and the density matrix, we get:

$$\frac{1}{2}\begin{pmatrix} \mathring{W}(t) & \mathring{z}(t) \\ \mathring{z}(t)^* & -\mathring{W}(t) \end{pmatrix} = \begin{pmatrix} -1/4\,i\left(\mathcal{E}(t)^* z(t) - \mathcal{E}(t) z(t)^*\right) & -1/2\,i\left(\mathcal{E}(t) W(t) + z(t)\omega_0\right) \\ 1/2\,i\left(\mathcal{E}(t)^* W(t) + z(t)^*\omega_0\right) & 1/4\,i\left(\mathcal{E}(t)^* z(t) - \mathcal{E}(t) z(t)^*\right) \end{pmatrix} \tag{22}$$

where the $\mathring{z}$ and $\mathring{W}$ are the temporal derivatives. We can then write:

$$\begin{cases} \mathring{z}(t) = -i\omega_0 z(t) - i\mathcal{E}(t)W(t) \\ \mathring{W}(t) = \dfrac{1}{2i}(\mathcal{E}(t)^* z(t) - \mathcal{E}(t) z(t)^*) \end{cases}. \tag{23}$$

Introducing relaxation mechanisms by $\gamma_1 = \frac{1}{T_1}$ and $\gamma_2 = \frac{1}{T_2}$ (respectively, the inverse of the decay time of the population difference and the inverse of the dipole dephasing time) and W_{eq}, the population difference at thermodynamic equilibrium, we get the generic form of the optical Bloch equations [8]:

$$\begin{cases} \mathring{z}(t) = -(\gamma_2 + i\omega_0) z(t) - i\mathcal{E}(t)W(t) \\ \mathring{W}(t) = -\gamma_1(W(t) - W_{eq}) + \dfrac{1}{2i}(\mathcal{E}(t)^* z(t) - \mathcal{E}(t) z(t)^*) \end{cases}. \tag{24}$$

Appendix 2. Transition Dipole Moment μ_{ab} for a Linear Molecule

Two orthonormal frames are introduced to discuss the dipole moment of a molecule. The first frame $(\vec{e}_x, \vec{e}_y, \vec{e}_z)$ is a laboratory-fixed frame. The second frame $(\vec{e}_X, \vec{e}_Y, \vec{e}_Z)$ is attached to the molecule.

The interaction of the molecule with the electric field $\vec{E}(y,t) = E_0(y,t)\,\vec{e}_z$ polarized along $\vec{e}_z$ is then described by the $-\vec{\hat{\mu}} \cdot E_0\,\vec{e}_z$ term.

We can decompose the dipole moment operator $\vec{\hat{\mu}}$ of the molecule in either the laboratory-fixed or the body-fixed frame:

$$\vec{\hat{\mu}} = \hat{\mu}_x\vec{e}_x + \hat{\mu}_y\vec{e}_y + \hat{\mu}_z\vec{e}_z = \hat{\mu}_X\vec{e}_X + \hat{\mu}_Y\vec{e}_Y + \hat{\mu}_Z\vec{e}_Z.$$

The interaction term is thus proportional to $\vec{\hat{\mu}} \cdot \vec{e}_z = \hat{\mu}_z = -\hat{\mu}_X\vec{e}_X \cdot \vec{e}_z + \hat{\mu}_Y\vec{e}_Y \cdot \vec{e}_z + \hat{\mu}_Z\vec{e}_Z \cdot \vec{e}_z$. For a linear molecule, $\hat{\mu}_X = \hat{\mu}_Y = 0$ if the nuclei of the atoms are on the Z-axis and the interaction term is then proportional to $\hat{\mu}_z = \vec{\hat{\mu}} \cdot \vec{e}_z = \hat{\mu}_Z\vec{e}_Z \cdot \vec{e}_z$ with $\vec{e}_Z \cdot \vec{e}_z = \cos\theta = \sqrt{\frac{4\pi}{3}}Y_{1,0}(\theta,\varphi)$ the direction cosine between the z-axis and the Z-axis and $Y_{1,0}(\theta,\varphi)$ is the spherical harmonic function.

The transition dipole moment is defined as $T_{j_1,m_1}^{j_2,m_2} = \langle j_2, m_2|\hat{\mu}_z|j_1, m_1\rangle$. $T_{j_1,m_1}^{j_2,m_2}$ is computed as follows:

$$\begin{aligned} T_{j_1,m_1}^{j_2,m_2} &= \sqrt{\frac{4\pi}{3}}\hat{\mu}_Z \int_0^{\pi}\int_0^{2\pi} Y_{j_2,m_2}(\theta,\varphi)^* Y_{1,0}(\theta,\varphi) Y_{j_1,m_1}(\theta,\varphi) \sin\theta d\theta d\varphi \\ &= (-1)^{m_2}\sqrt{\frac{4\pi}{3}}\hat{\mu}_Z \int_0^{\pi}\int_0^{2\pi} Y_{j_2,-m_2}(\theta,\varphi) Y_{1,0}(\theta,\varphi) Y_{j_1,m_1}(\theta,\varphi) \sin\theta d\theta d\varphi \\ &= (-1)^{m_2}\sqrt{\frac{4\pi}{3}}\sqrt{\frac{3(2j_2+1)(2j_1+1)}{4\pi}} \begin{pmatrix} j_2 & 1 & j_1 \\ -m_2 & 0 & m_1 \end{pmatrix} \begin{pmatrix} j_2 & 1 & j_1 \\ 0 & 0 & 0 \end{pmatrix} \hat{\mu}_Z \\ &= (-1)^{m_2}\sqrt{(2j_2+1)(2j_1+1)} \begin{pmatrix} j_2 & 1 & j_1 \\ -m_2 & 0 & m_1 \end{pmatrix} \begin{pmatrix} j_2 & 1 & j_1 \\ 0 & 0 & 0 \end{pmatrix} \hat{\mu}_Z \end{aligned}$$

The transition dipole moment is zero if $m_1 \neq m_2$ due to the $3jm$ coefficient $\begin{pmatrix} j_2 & 1 & j_1 \\ -m_2 & 0 & m_1 \end{pmatrix}$. We define an averaged transition dipole moment as:

$$\left\langle T_{j_1,m_1}^{j_2,m_2}\right\rangle = \frac{1}{2j_1+1}\sum_{m=-j_1}^{m=j_1} T_{j_1,m}^{j_2,m} = \sqrt{\frac{2j_2+1}{2j_1+1}} \begin{pmatrix} j_2 & 1 & j_1 \\ 0 & 0 & 0 \end{pmatrix} \hat{\mu}_Z \sum_{m=-j_1}^{m=j_1} (-1)^m \begin{pmatrix} j_2 & 1 & j_1 \\ -m & 0 & m \end{pmatrix}. \tag{25}$$

For example, the permanent dipole moment of OCS is $\mu_Z = 0.70\,\mathrm{D}$ [21] and the transition dipole moment for the $J = 17 \rightarrow 16$ rotational transition is calculated to $\mu_{ab} = 0.28\,\mathrm{D}$ according to Eq. 25.

References

1. G.G. Brown, B.C. Dian, K.O. Douglass, S.M. Geyer, B.H. Pate, J. Mol. Spectrosc. **238**, 200 (2006).
2. G.G. Brown, B.C. Dian, K.O. Douglass, S.M. Geyer, S.T. Shipman, B.H. Pate, Rev. Sci. Instrum. **79**, 53103 (2008).
3. E. Gerecht, K.O. Douglass, D.F. Plusquellic, Opt. Express **19**(9), 8973 (2011).
4. G.B. Park, A.H. Steeves, K. Kuyanov-Prozument, J.L. Neill, R.W. Field, J. Chem. Phys. **135**(2), 024202 (2011).
5. A.L. Steber, B.J. Harris, J.L. Neill, B.H. Pate, J. Mol. Spectrosc. **280**, 3 (2012).
6. C. Abeysekera, B. Joalland, N. Ariyasingha, L.N. Zack, I.R. Sims, R.W. Field, A.G. Suits, J. Phys. Chem. Lett. **6**(9), 1599 (2015).
7. F. Hindle, C. Bray, K. Hickson, D. Fontanari, M. Mouelhi, A. Cuisset, G. Mouret, R. Bocquet, J. Infrared Millim. Te. **39**(1), 105 (2018).
8. D. Fontanari, C. Bray, G. Dhont, G. Mouret, A. Cuisset, F. Hindle, R. Bocquet, K.M. Hickson, Phys. Rev. A **100**, 043407 (2019).
9. J.C. McGurk, T.G. Schmalz, W.H. Flygare, J. Chem. Phys. **60**(11), 4181 (1974).
10. H. Mäder, H. Bomsdorf, U. Andresen, Z. Naturforsch. **34a**, 850 (1979).
11. T.J. Balle, W.H. Flygare, Rev. Sci. Instrum. **52**(1), 33 (1981).
12. D. Boucher, R. Bocquet, D. Petitprez, L. Aimé, Int. J. Infrared Milli. **15**(9), 1481 (1994).
13. R. Bocquet, X. Li, L. Aimé, D. Petitprez, D. Boucher, Int. J. Infrared Milli. **16**(2), 445 (1995).
14. J.C. McGurk, T.G. Schmalz, W.H. Flygare, *Advances in chemical physics* (John Wiley & Sons, Ltd, 1974), vol. XXV, chap. 1, pp. 1–68.
15. M. Broquier, C. Crépin, H. Dubost, J.P. Galaup, Chem. Phys. **341**, 207 (2007).
16. A. Materny, T. Chen, M. Schmitt, T. Siebert, A. Vierheilig, V. Engel, W. Kiefer, Appl. Phys. B **71**(3), 299 (2000).
17. F. Rohart, B. Macke, Appl. Phys. B **26**(1), 23 (1981).

18. M.D. Levenson, S.S. Kano, *Introduction to nonlinear laser spectroscopy* (Academic Press Inc, 1988).
19. P. Meystre, M. Sargent III, *Elements of quantum optics 3rd edition* (Springer, 1999).
20. G.B. Park, R.W. Field, J. Chem. Phys. **144**(20), 200901 (10 pages) (2016).
21. S. Matton, F. Rohart, R. Bocquet, G. Mouret, D. Bigourd, A. Cuisset, F. Hindle, J. Mol. Spectrosc. **239**(2), 182 (2006).
22. F. Merkt, M. Quack, *Handbook of high-resolution spectroscopy* (Wiley and Sons, 2011), vol. 1 - Fundamentals and Theory, pp. 1–55.